

Active Vapor-Based Robotic Wiper

Takuya Kiyokawa*, Hiroki Katayama, and Jun Takamatsu

Abstract—This paper presents a method for the normal estimation of mirrors and transparent objects that are difficult to recognize with a camera. To create a diffuse reflective surface, we propose spraying water vapor onto transparent or mirror surfaces. In the proposed method, we move an ultrasonic humidifier equipped on the tip of a robotic arm to apply sprayed water vapor onto the plane of a target object to form a cross-shaped misted area. Diffuse reflective surfaces are partially generated as misted areas, which allows the camera to detect the surface of the target object. The viewpoint of the gripper-mounted camera is adjusted such that the extracted misted area appears to be the largest in the image, and finally, the plane normal of the target object surface is estimated. Normal estimation experiments were conducted to evaluate the effectiveness of the proposed method. The RMSEs of the azimuth estimation for the mirror and transparent glass were approximately 4.2° and 5.8° , respectively. Consequently, our robot experiments demonstrate that our robotic wiper can perform contact-force-regulated wiping motions to clean a transparent window, as humans do.

Index Terms—Transparent, Mirror, Active Vapor, Normal Estimation, Wiping, Service Robot

I. INTRODUCTION

OWING to the increase in the number of elderly persons living alone and the labor shortage, researchers have studied household robots performing various houseworks [1], [2], such as window-wiping [3], [4] and water-pouring [5]–[7]. To expand the use of robots in home environment applications, it is necessary to recognize more diversified objects than ever before. The robot must robustly recognize any type of target object surface to make accurate contact with fragile household objects so that the robot gripper does not damage or break the target object.

In particular, optical cameras are difficult to capture the plane normal of a mirror and a transparent object without any diffuse reflection surfaces because specular reflection or light transmission occurs on non-Lambertian surfaces [8]. To clean the window or mirror surfaces using a home robot, we need to achieve a robotic system that can recognize and wipe them without using the automatic wiping-specific machines previously proposed [9]–[13].

In this study, we propose to spray water vapor on such surfaces. As a result, we can control the visibility of the mirror and transparent surfaces, and then estimate their plane normals. First, we developed a robotic wiper system based on the *Active Vapor* method as shown in Fig. 1. Second, the robot system generates a cross-shaped misted area by actively spraying water vapor onto the target plane using an ultrasonic

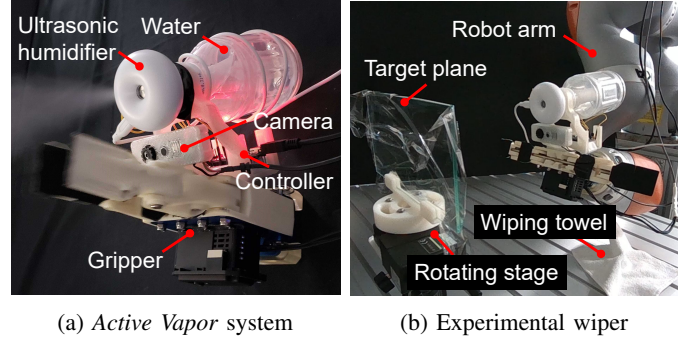


Fig. 1: Robotic window-wiping system based on *Active Vapor*. The system has three functions: spraying water vapor, grasping an object, and capturing an image.

humidifier attached to a gripper mounted on the robot arm. Third, the robot wipes based on the estimated plane normal with contact-force-regulated linear motions.

In our experiments, the developed robotic wiper performed plane normal estimation for a mirror and transparent glass and contact-regulated wiping motion to clean a mirror and a transparent window. The proposed method can estimate the azimuth angle with small errors of less than 4.2° and 5.8° for a mirror and transparent glass, respectively.

This study makes three contributions.

- 1) To the best of our knowledge, we first present an *Active Vapor* method that creates a cross-shaped misted area for transparent objects and mirrors by spraying water vapor while moving a robot arm.
- 2) The experimental results show that the azimuth angle can be estimated with an accuracy of approximately 6° or less in a real environment subject to physical constraints, such as the time until the water vapor disappears.
- 3) We comprehensively discuss the limitations and future improvements of this novel sensing for non-Lambertian surfaces. Concretely, we summarize other types of water vapor, contact control methods, dependencies at room temperature, and improved normal estimation.

II. RELATED WORKS

A. Vision-Based Approach

Different approaches have been proposed for recognizing mirrors and transparent objects. The previous studies in the field of physics-based vision tackled several methods for observing and analyzing the polarization state of light reflected on and transmitted from object surfaces [14], [15], extracting and analyzing highlights on a transparent object surface [16],

All authors are with Division of Information Science, Nara Institute of Science and Technology (NAIST), Japan. T. Kiyokawa is with Department of Systems Innovation, Osaka University, Japan. J. Takamatsu is with the Applied Robotics, Microsoft, US. *kiyokawa.takuya@is.naist.jp

Digital Object Identifier (DOI): see top of this page.

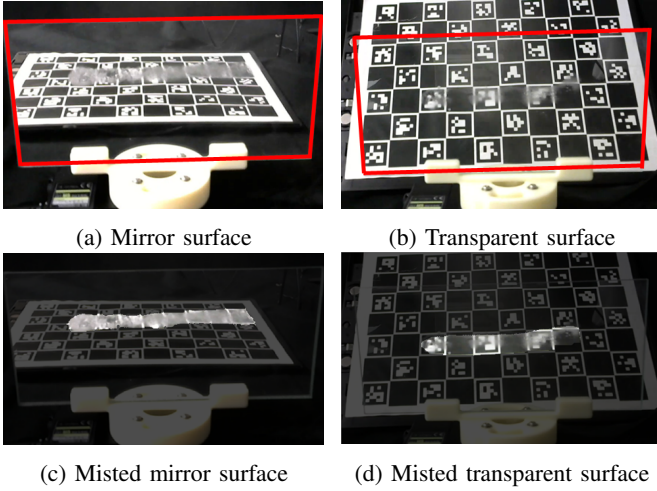


Fig. 2: Misted-area appearance. We applied image segmentation (e.g., *GrabCut* [38]) to extract the areas of a mirror and transparent glass. The red lines indicate the outlines of the mirror and glass.

analyzing the refraction of the background through a transparent object [17], [18], and recognizing deflections by projecting a pattern on a mirror surface [19].

Another learning-based method used latent features of the appearance of transparent objects that does not depend on the background [20]. Other studies used a failure area of depth images [21]–[23].

Current robot-vision systems have enabled the recognition of mirrors and transparent objects using previous methods. Robot manipulators have been able to grasp them, while mobile robots can avoid them [24]–[27]. Recent studies have used deep learning to extract latent characteristics of transparent objects from large amounts of training data [28]–[32]. Few studies have attempted to recognize washstand mirrors and transparent glass windows, which have no other objects in the background or vicinity of the object and often have little reflection.

B. Sound-Based Approach

Several studies have attempted object recognition using sound instead of light [4]. Transparent objects have been classified using ultrasound [33]. Even with sound signals, depth can be obtained using time-of-flight (TOF) method, but the resolution is difficult to improve. Different sound-based approaches using arrayed sensors have been used to restore a depth image with a resolution of approximately 30×30 [34] and to recognize hand shapes using distance information [35].

However, even if arrayed ultrasonic sensors are used, sound signals still have a low spatial resolution. Although reflective sound lines can be used to recognize the indoor environment [36], modeling diffraction phenomena and sound reflection have been used to recognize the surrounding environment [37]. However, these sound-based methods are still difficult to apply in noisy environments.

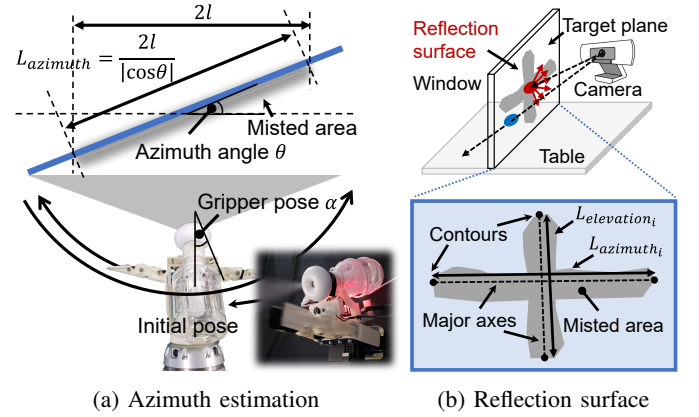


Fig. 3: Normal estimation method. (a) shows an overview of the gripper motion and geometries between the gripper and misted plane. The top part of (b) shows the reflection surface that appears on the target plane. The bottom part of (b) shows the geometry of the cross-shaped misted area viewed from viewpoint i .

III. ACTIVE VAPOR-BASED NORMAL ESTIMATION

A. Estimating Normal Direction from Misted Cross-Shape

The misted surface appearances of the mirror and transparent glass are shown in Fig. 2 (a) and (b), respectively. The misted area was diffusely reflected because it became blurred. Therefore, the misted area appears to be different from the surrounding area. By making a cross-shaped area the misted area, we can estimate the normal direction from the line segment lengths, so it is not very important to produce accurate boundaries. Because a certain vapor-covered line segment can be used to estimate the normal sufficiently, a traditional image segmentation method is desirable.

The azimuth angle θ and elevation angle ϕ can be estimated based on the geometries between the tilt angle of the target plane and the misted area sprayed with a cross shape. Because the azimuth and elevation angles can be calculated in the same way, the calculation of the azimuth angle is described as an example. Fig. 3 (a) shows the geometry of the azimuth angle. If the lengths of both the vertical and horizontal axes in the cross-shaped misted area are $2l$, set by the length of the robot arm trajectory, then the angle value is calculated as follows:

$$\theta = \pm \cos^{-1} \frac{2l}{L_{azimuth}}. \quad (1)$$

However, this solution is not uniquely determined. Therefore, it is assumed that the calculated length of the misted area $L_{azimuth_i}$ is the maximum when the target plane is perpendicular to the image-capturing direction of the camera.

Based on this geometric constraint, the azimuth angle is estimated. First, by moving the viewpoint of the camera with the robot arm after completing the water vapor spraying, we determine the direction of the camera viewpoint i , where $L_{azimuth_i}$ ($i = 1, 2, \dots, n$) is the maximum, where n is the number of viewpoint positions changed by the motion of the robot arm. Second, the angle between the estimated and initial directions before moving is determined as the estimated azimuth $\hat{\theta}$.

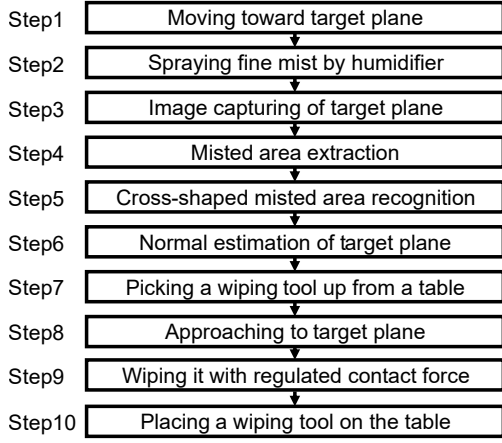


Fig. 4: Basic steps. Normal estimation of mirror planes and transparent objects.

As shown in the top part of Fig. 3 (b), $L_{azimuth_i}$ is obtained as follows. First, we calculate the intersections of the longest (major) axes and the contours of the misted area. Second, we calculate the distance between intersections as $L_{azimuth_i}$.

Given the estimated elevation angle as $\hat{\phi}$, the normal \mathbf{N} at the initial position of the sprayed plane is calculated as

$$\mathbf{N} = (\cos \hat{\phi} \cos \hat{\theta}, \cos \hat{\phi} \sin \hat{\theta}, \sin \hat{\phi}). \quad (2)$$

B. Spraying Water Vapor

Fig. 4 shows an outline of the proposed method. We start spraying water vapor at the point where the robot gripper approaches the target plane. The position of the sprayed water vapor is changed by the robot arm motion to mark a misted area in the shape of a cruciform shape.

To determine both the azimuth and elevation angles from the extracted line lengths, the system creates a cross-shaped misted area on the target surface. To obtain the cross-shaped misted area, in the spraying motion, the robot arm performs a reciprocating motion of linear trajectories up/down and left/right from the initial position where the robot has approached the target plane. After completing the spraying, the robot arm moves on the arcs of the radius of the distance from the initial position to the target plane in both the directions of elevation and azimuth displacement. The circumferential speed at which the robot moves on the arc is generated such that it takes less time than $T_{completion}$ [s] to complete the movement on the arc; thus, the following equation is satisfied:

$$\frac{r\beta}{v_{wrist}} < T_{completion}, \quad (3)$$

where r [mm] is the distance to the target plane, β [rad] is the rotation angle of the robot gripper when estimating the normal after completing the water vapor spraying, and v_{wrist} [mm/s] is the circumferential speed at that time.

IV. WINPING SYSTEM IMPLEMENTATION

A. Active Vapor System

Fig. 1 (a) shows the appearance of the robot gripper equipped with a sensing system based on Active Vapor. Fig. 5

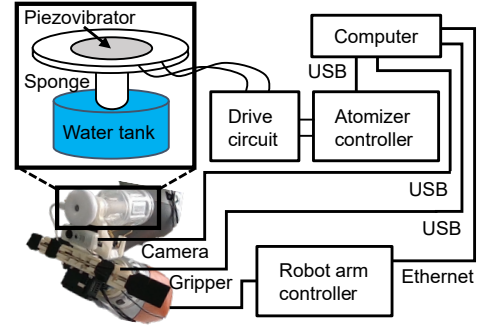


Fig. 5: Hardware architecture diagram. An ultrasonic humidifier can spray water vapor by vibrating the piezovibrator, where a sponge is pressed against the other side of the vibrator. The sponge absorbs water from the water tank. To toggle the piezovibrator, we command atomizer controller from the computer. The robot arm, gripper, and camera are controlled using the same computer.

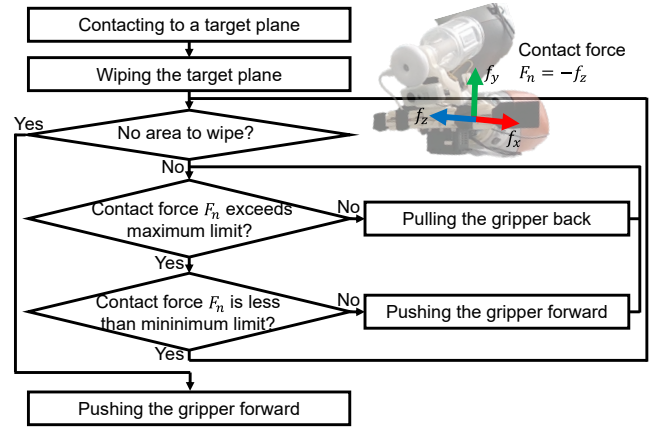


Fig. 6: Contact force regulation process. A simple adjustment is made to keep the contact force as constant as possible (this is not the main focus of the study).

shows the hardware architecture the proposed system. We use a two-fingered gripper (SAKE Robotics, EZGripper) as the end-effector to enable the robot system to grasp a target wiping tool, such as a washcloth or sponge. A small ultrasonic humidifier is used to atomize and eject the water. When the built-in vibrator vibrates slightly due to ultrasonic waves, the water on the contact surface with the sponge sucked from the bottle is atomized and ejected from the donut-shaped tip. An RGB camera is attached to the bottom of the gripper to capture the target plane misted by ejected water vapor. The resolution of the camera was HD (1280 x 720) and the frame rate was 30 fps. All the devices are controlled by the same computer, as shown in Fig. 5.

The target plane is captured by the camera and the misted area on the plane is extracted using *GrabCut* [38]. The (c) and (d) of Fig. 2 show the images of misted surface of a mirror and a transparent glass. In the wiping experiments, for the misted area extracted as the foreground after the *GrabCut* processing, the shape of the misted area is extracted as a cross shape, and the normal of the misted surface is estimated based on the shape.

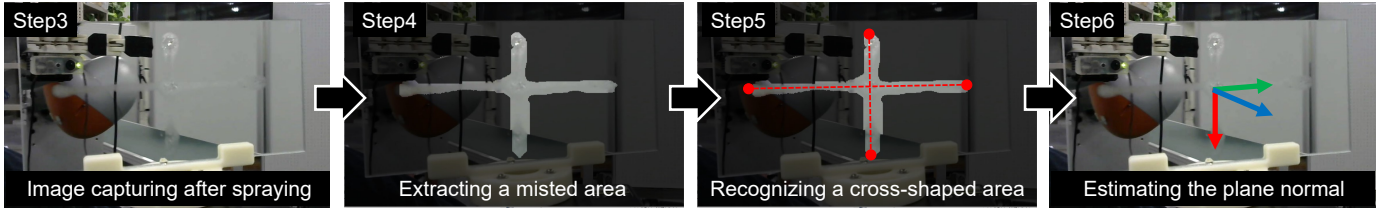


Fig. 7: Normal estimation process. In our experiments, the system estimated a misted area on the mirror surface. The step numbers shown at the top left of the images correspond to those shown in Fig. 4.

B. Contact-Regulated Robotic Wiper

If stable contact with the target object surface cannot be achieved, the dirt on the surface cannot be wiped off cleanly. We do not control the contact force directly but regulate the contact force with an effective contact force range defined with minimum and maximum normal force thresholds of 3.0 and 8.0 [N], respectively, which are empirically determined. Fig. 6 shows an overview of the simple force-regulation process. The normal force F_n is calculated as $-f_z$ which represents the contact force in the z-axis direction.

The experiments were performed using a contact-force-regulated robotic wiping system. The contact force f_z is obtained as the force in the z-axis direction of the three-axis force on the arm-wrist coordinate system, as shown in Fig. 6. These were calculated from the torque sensors inside the six joints of the arm. We can easily obtain the force values in *iiwa_stack*¹, which is the ROS metapackage for the robot arm (KUKA, LBR iiwa 14 R820) used in our experiments.

V. EXPERIMENTS

A. Overview

To evaluate the effectiveness of the proposed Active Vapor method, we conducted a plane normal estimation for a mirror and transparent glass window. Fig. 1 (b) shows the experimental system. The developed sensor system is attached to the flange of a single robot arm, which has seven degrees of freedom that can be controlled over a wide range of viewpoint positions.

To efficiently perform the experiments, we used an automatic rotating stage to change the azimuth angle of the target plane. We used a mirror and transparent glass with a thickness of 3mm because the proposed system cannot place water vapor on the target surfaces when the plane's thicknesses are more than 3mm. The maximum thickness at which the misted area could be generated on both the mirror and the glass was 3mm.

To simplify the evaluation process, only the azimuth angle was estimated. The azimuth angle was varied in three patterns of -20° , 0° , and 20° . We conducted three trials for all three patterns for each target object.

It was difficult to generate a misted area by spraying water vapor when the distance from the target plane was greater than 100mm. To bring the sensor close enough to the target surface while avoiding collision, we set $r = 100\text{mm}$ as the maximum distance at which the misted area could be generated. From the initial position, where $r = 100\text{mm}$, the robot performed

the linear motion of three reciprocations in the vertical and horizontal directions.

We performed ten trial spraying operations to evaluate the time from spraying water vapor until the misted area disappeared. In the experiments, the temperatures inside the room, outside the room, and inside the bottle were 23°C , 26°C , and 22°C , respectively. As a result, the misted area began to disappear within approximately 6s at the fastest rate.

Based on the preliminary result, the trajectory of the gripper was generated as a circular arc during normal estimation and was completed in a time shorter than $T_{\text{completion}} = 6$ [s]. In this experiment, to complete the spraying motion with image capturing before the misted area disappeared, we set 50mm/s as the speed of the robot gripper motion v_{wrist} . This speed was more than twice as fast as the lowest speed of 17mm/s calculated using Equation (3) with $r = 100$ [mm] and $\beta = 60 \times \pi / 180$ [rad].

B. Plane Normal Estimation Accuracy

We trained the extraction model of GrabCut using 100 images captured in the same environment as the experiments.

The RMSE of the estimation in the azimuth range from -20° to 20° was calculated. They were 4.2° and 5.8° for the mirror and transparent glass window, respectively. From these results, even when the proposed Active Vapor-based sensing system is attached to the robot, the plane normal can be estimated accurately.

Consequently, the estimation error on the mirror surface was smaller than the error on the transparent object surface. This is probably because we experimented in a laboratory; there were few characteristic objects in the background of transparent objects, and it was difficult to extract the misted area itself.

In contrast, in the case of a mirror surface, a robot gripper or robot arm was reflected, as shown in Fig. 7, and there were multiple objects with visual characteristics. We believe that the misted area was learned as the foreground by GrabCut from the refraction of the appearance.

C. Evaluating Window Wiping

1) *Wiping Accuracy*: We evaluated the performance of wiping as follows. First, we manually painted the water-based blue ink on a predefined area of the window. The painted area was approximately 15cm long and 2cm wide. Second, the robot executed the wiping motion of three round trips along a straight line, as partially shown in Fig. 8. Finally, we estimated the area of the ink remaining after the wiping motion. We defined the performance as A_{unwiped} [mm²].

¹https://github.com/IFL-CAMP/iiwa_stack

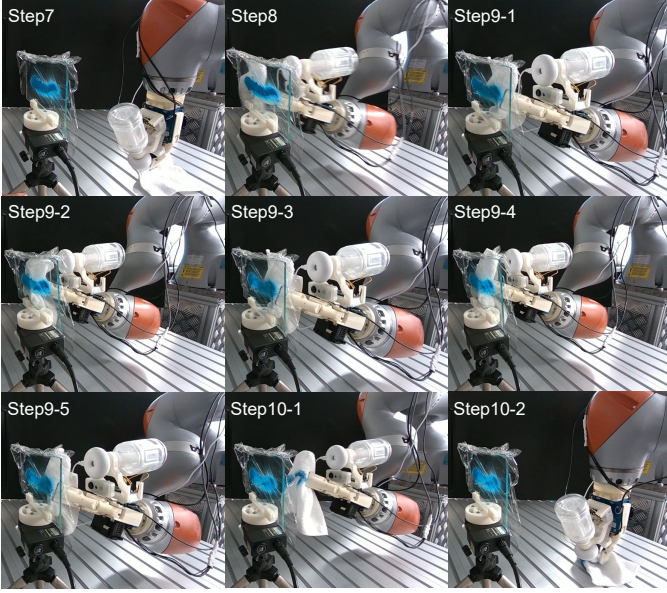


Fig. 8: Wiping motion. We generate the initial linear motions to wipe, which are slanted with estimation errors [$^{\circ}$]. Subsequently, the gripper contacted the target object and the three reciprocating wiping motions were executed while the contact force was regulated. The step numbers correspond to those shown in Fig. 4.

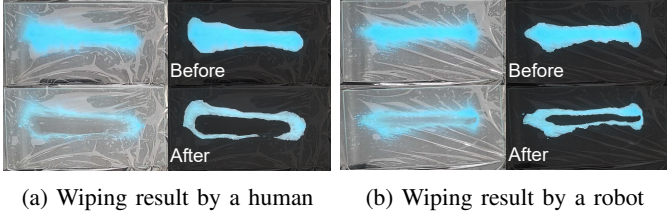


Fig. 9: Ink-stained windows before and after wiping. Both (a) and (b) show the windows before a wiping motion (top left), the result of segmenting the blue from the background (top right), the window after the wiping (bottom left), and the result (bottom right).

We verified the relationship between the quality of the window-wiping operation and the error in the azimuth angle estimation. The area unwiped by the robot $A_{unwiped}$ [mm²] is calculated as

$$A_{unwiped} = A_{initial} \times \frac{N_{final}}{N_{initial}}, \quad (4)$$

where $A_{initial}$ [mm²] is the measured ink-stained area, which is set to 5000 mm², $N_{initial}$ and N_{final} represent the number of pixels of the ink-stained area before and after the wiping motion, respectively.

The end effector was moved along a straight line. Fig. 8 shows the sequence of the wiping experiments. The ink-stained area in the image was extracted using GrabCut. We evaluated the case of a human wiping operation and the case of a robot wiping operation with a 5.8 $^{\circ}$ error. We compare the two cases on the calculated wiped area α [%] formulated as

$$\alpha = \frac{(A_{initial} - A_{unwiped})}{A_{initial}} \times 100. \quad (5)$$

Fig. 9 shows the experimental results. When the azimuth angle estimation error was 5.8 $^{\circ}$ for the transparent glass

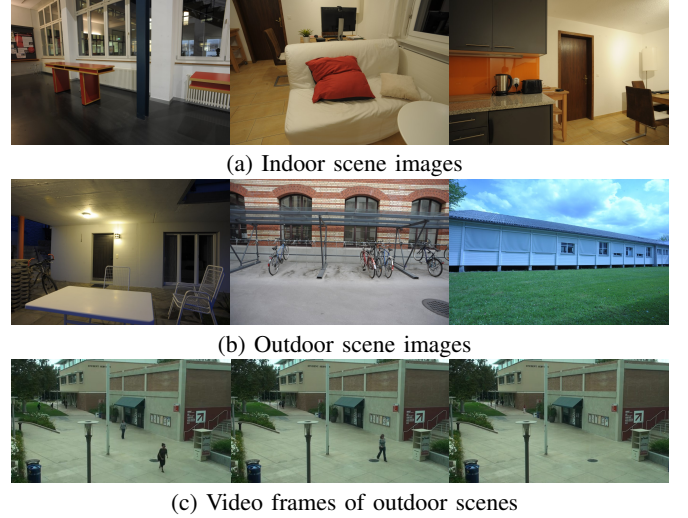


Fig. 10: Background scenes. We used them to evaluate the robustness of the proposed misted-area extraction.

window, the mean of the α in three trials was 45.2%. The regulated contact force of the robot gripper made the robot wiping motions more accurate when cleaning the ink-stained plane. The α was improved to 52.2%. When the human performed, the mean of the α in three trials was 65.1%. Therefore, if we can use the estimation result with an error of 5.8 $^{\circ}$, we can remove approximately 52.2% of the ink.

2) *Wiping Efficiency*: To evaluate the efficiency of the proposed wiping system, we investigated how much can we shorten the time to complete the wiping operations.

We experimented with normal estimation with several spraying and image-capturing motions in a shorter time. Our experiments demonstrated that the one-way spraying motion for less than 2s tend to fail. Failure was defined as a misted area of almost zero, which was checked by human visual inspection. Although the frame rate of the camera depends on the result, the image capturing motions in less than 3s tend to fail. A camera with a frame rate of 30 fps was used.

3) *Wiping Effectiveness*: To validate the effectiveness of the proposed wiping system, we compared its wiping accuracies. Because it was not possible to extract the misted areas well depending on the reflected scene and background, we validated the robustness of the proposed normal estimation for various backgrounds in the case of a transparent window.

We show the experimental results by comparing the extraction accuracy of misted areas between different background types for a transparent glass window. We experimented with several indoor and outdoor scenes as the background. We extracted indoor (room) and outdoor (garden and sky) images from the *ETH3D Stereo Benchmarks* [39] and extracted outdoor videos from the *VIRAT Video Dataset* [40]. We used three images of different indoor scenes, three images of different outdoor scenes, and three video frames of outdoor scenes. Fig. 10 shows examples of the images used in the experiment.

Fig. 11 shows a comparison of misted area extraction using different backgrounds. We calculated F-scores to evaluate the accuracy of the segmentation of misted areas using manually

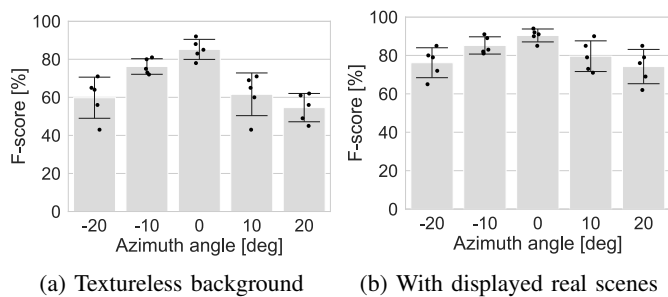


Fig. 11: Comparison of misted-area extraction from different backgrounds. Both (a) and (b) show the extraction results (F-scores). We annotated five images for each angle as the ground truth and calculated the F-scores using the extracted misted areas of the ground truth data and the extraction results.

annotated ground truth segmentation data with an image annotation tool called *labelme*². We annotated five images for each angle and calculated the F-scores using the extracted misted areas of the ground truth data and the extraction results using our proposed method. As a result, the normal estimation error was 5.0° which is slightly lower but similar to the normal estimation of the transparent glass plane with a textureless background. However, the misted area extraction was more robust to the viewpoint than the textureless background.

VI. DISCUSSION

1) *Other Types of Vapor*: To improve the accuracy of the normal estimation, we thought that the painted water vapor could be used because the painted area could be identified more clearly, and we thought we could use a detergent, not limited to water vapor, in that it can be cleaned later even if it becomes dirty.

As shown in Fig. 12, we can spray water colored with water-based food colors, but it is difficult to spray visible colored vapor on the target surfaces. If oil-based paint is used, it is difficult for the ultrasonic humidifier to output the oil-based paint and the surface will be stained with the sprayed oil.

Using a liquid containing a detergent for window wiping is dangerous and cannot be easily attempted. Several types of detergents can be harmful to the human body if they breathe through the nose or mouth. Therefore, in this study, to ensure human safety, we did not try to use detergents.

2) *Controlling Contact*: The accuracy and efficiency of the wiping motions depend on the stable contact between the robot gripper and the target surface to be wiped. The contact-force controller can be used for more flexible motion.

Leidner *et al.* [41] tackled the automation of robot wiping motions with the whole body motion control. Luo *et al.* [42] enabled users to easily adjust the end-effector's force setpoint while commanding the end-effector motion to successfully execute the task. In this study, force control methods are beyond the scope of this study, but we can refer to these studies to achieve a flexible wiping motion. If we control the contact force precisely, the time required for the motion tends to be longer than that without control. In our future work, referring



(a) Misted glass with red water (b) Misted glass with blue water

Fig. 12: Surfaces sprayed of colored water vapor. We colored the water and saturated the sponge inside the humidifier with colored water. The humidifier then sprayed water vapor.

to other studies [43], we will tackle a control method and re-estimation method of plane normal while reducing the motion time.

3) *Temperature*: It is possible to obtain an adequate misted area to estimate the normal depending on the saturated water vapor content. To confirm the relationship between room temperature and time to dry the crossed misted area, we tried three conditions for the room temperature: 20°C , 25°C , and 30°C with the same humidity of 65%.

Five spraying trials were conducted for each temperature. The average times of the trials for the three temperature conditions were 92s, 74s, and 68s respectively. There are few differences between them, but they are not significantly different.

4) *Improved Normal Estimation*: Because it is not possible to extract the misted areas well depending on the reflected scene and the background, we can consider building an algorithm that carefully looks at what is reflected and can be seen on the background and selects where to spray it.

In addition, there is room to discuss a method for generating the minimum trajectory that can be completed before the misted areas are dried out. In this study, we apply a cross-shaped misted area on the target surface, but it takes a long time to make the cross-shape, so we can reduce the time for the motions by optimizing the motions in our future study.

In this study, we concentrate on the plane normal estimation, but the normal estimation for curved surfaces is based on light-field features [44], [45], which would be a promising direction for future studies.

VII. CONCLUSIONS

In this paper, we propose a method for the normal estimation of mirrors and transparent objects that are difficult to recognize with a camera. In the proposed method, a sensor system attached to the robot arm is used to wipe the target object. Water vapor was sprayed in the direction of the target plane to generate a cross-shaped misted area. The plane normal was estimated by extracting the misted area using GrabCut. Experiments on normal estimation for a mirror and a transparent glass window using the proposed system showed an average error of 4.2° and 5.8° for the surfaces of the mirror and transparent glass window, respectively.

In future work, we will improve the estimation system and conduct experiments that consider various objects in home environments. Furthermore, we will construct a contact-controlled robotic window-cleaning system that is robust for

²<https://github.com/wkentaro/labelme>

any poses on the target object surface even if there are normal estimation errors.

REFERENCES

- [1] P. Fiorini and E. Prassler, "Cleaning and household robots: A technology survey," *Auton. Robots*, vol. 9, pp. 227–235, 2000.
- [2] N. Wake, R. Arakawa, I. Yanokura, T. Kiyokawa, K. Sasabuchi, J. Takamatsu, and K. Ikeuchi, "A learning-from-observation framework: One-shot robot teaching for grasp-manipulation-release household operations," in *SI*, 2021, pp. 461–466.
- [3] D. Leidner, A. Dietrich, M. Beetz, and A. Albu-Schäffer, "Knowledge-enabled parameterization of whole-body control strategies for compliant service robots," *Auton. Robots*, vol. 40, pp. 519–536, 2016.
- [4] H. Katayama, T. Kiyokawa, J. Takamatsu, and T. Ogasawara, "Azimuth angle estimation based on sound wave reflection for mirrors and transparent objects," in *SI*, 2021, pp. 40–45.
- [5] C. Schenck and D. Fox, "Visual closed-loop control for pouring liquids," in *ICRA*, 2017, pp. 2629–2636.
- [6] T. Kiyokawa, M. Ding, G. A. G. Ricardez, J. Takamatsu, and T. Ogasawara, "Generation of a tactile-based pouring motion using fingertip force sensors," in *SI*, 2019, pp. 669–674.
- [7] Y. Tsuchiya, T. Kiyokawa, G. A. Garcia Ricardez, J. Takamatsu, and T. Ogasawara, "Pouring from deformable containers using dual-arm manipulation and tactile sensing," in *IRC*, 2019, pp. 357–362.
- [8] F. Meriaudeau, R. Rantson, D. Fofi, and C. Stolz, "Review and comparison of non-conventional imaging systems for three-dimensional digitization of transparent objects," *J. Electron. Imaging*, vol. 21, no. 2, pp. 1–6, 2012.
- [9] T. Miyake and H. Ishihara, "Mechanisms and basic properties of window cleaning robot," in *AIM*, vol. 2, 2003, pp. 1372–1377.
- [10] T. Miyake, H. Ishihara, R. Shoji, and S. Yoshida, "Development of small-size window cleaning robot a traveling direction control on vertical surface using accelerometer," in *ICMA*, 2006, pp. 1302–1307.
- [11] N. Imaoka, S.-g. Roh, N. Yusuke, and S. Hirose, "SkyScraper-I: Tethered whole windows cleaning robot," in *IROS*, 2010, pp. 5460–5465.
- [12] J. Hong, T. Kim, H. Chae, G. Park, J. Lee, J. Kim, H. S. Kim, and T. Seo, "Design of window-cleaning robotic manipulator with compliant adaptation capability," *IEEE/ASME Trans. Mechatron.*, vol. 25, no. 4, pp. 1878–1885, 2020.
- [13] Z. Li, Q. Xu, and L. M. Tam, "A survey on techniques and applications of window-cleaning robots," *IEEE Access*, vol. 9, pp. 111 518–111 532, 2021.
- [14] D. Miyazaki, M. Kagesawa, and K. Ikeuchi, "Transparent surface modeling from a pair of polarization images," *IEEE PAMI*, vol. 26, no. 1, pp. 73–82, 2004.
- [15] D. Miyazaki and K. Ikeuchi, "Shape estimation of transparent objects by using inverse polarization raytracing," *IEEE PAMI*, vol. 29, no. 11, pp. 2018–2030, 2007.
- [16] K. McHenry, J. Ponce, and D. Forsyth, "Finding glass," in *CVPR*, 2005, pp. 973–979.
- [17] M. Yamazaki, S. Iwata, and G. Xu, "Dense 3D reconstruction of specular and transparent objects using stereo cameras and phase-shift method," in *ACCV*, 2007, pp. 570–579.
- [18] Y. Xu, H. Nagahara, A. Shimada, and R. Taniguchi, "Transcut2: Transparent object segmentation from a light-field image," *IEEE Trans. Comput. Imaging*, vol. 5, no. 3, pp. 465–477, 2019.
- [19] T. Zhou, K. Chen, H. Wei, and Y. Li, "Improved method for rapid shape recovery of large specular surfaces based on phase measuring deflectometry," *Applied Optics*, vol. 55, no. 10, pp. 2760–2770, 2016.
- [20] M. Fritz, M. Black, G. Bradski, S. Karayev, and T. Darrell, "An additive latent feature model for transparent object recognition," in *NIPS*, 2009, pp. 558–566.
- [21] C. J. Phillips, K. G. Derpanis, and K. Daniilidis, "A novel stereoscopic cue for figure-ground segregation of semi-transparent objects," in *ICCV Workshops*, 2011, pp. 1100–1107.
- [22] I. Lysenkov, V. Eruhimov, and G. Bradski, "Recognition and pose estimation of rigid transparent objects with a kinect sensor," in *RSS*, 2012.
- [23] R. C. Luo, P. Lai, and V. W. S. Ee, "Transparent object recognition and retrieval for robotic bio-laboratory automation applications," in *IROS*, 2015, pp. 5046–5051.
- [24] U. Klank, D. Carton, and M. Beetz, "Transparent object detection and reconstruction on a mobile platform," in *ICRA*, 2011, pp. 5971–5978.
- [25] V. R. Kompella and P. Sturm, "Detection and avoidance of semi-transparent obstacles using a collective-reward based approach," in *ICRA*, 2011, pp. 3469–3474.
- [26] K. O. Z. Lei, M. Tsubota, E. Takeuchi, and S. Tadokoro, "Transparent object detection using color image and laser reflectance image for mobile manipulator," in *ROBIO*, 2011, pp. 1–7.
- [27] C. J. Phillips, M. Lecce, and K. Daniilidis, "Seeing Glassware: from edge detection to pose estimation and shape recovery," in *RSS*, 2016.
- [28] X. Liu, R. Jonschkowski, A. Angelova, and K. Konolige, "KeyPose: Multi-view 3D labeling and keypoint estimation for transparent objects," in *CVPR*, 2020, pp. 11 602–11 610.
- [29] S. S. Sajjan, M. Moore, M. Pan, G. Nagaraja, J. Lee, A. Zeng, and S. Song, "ClearGrasp: 3D shape estimation of transparent objects for manipulation," in *ICRA*, 2020, pp. 3634–3642.
- [30] L. Zhu, A. Mousavian, Y. Xiang, H. Mazhar, J. van Eenbergen, S. Debnath, and D. Fox, "RGB-D local implicit function for depth completion of transparent objects," in *CVPR*, 2021, pp. 4649–4658.
- [31] Y. Tang, J. Chen, Z. Yang, Z. Lin, Q. Li, and W. Liu, "DepthGrasp: Depth completion of transparent objects using selfattentive adversarial network with spectral residual for grasping," in *IROS*, 2021, pp. 5687–5693.
- [32] J. Chang, M. Kim, S. Kang, H. Han, S. H. Kyunghun, and J. S. Kang, "GhostPose*: Multi-view pose estimation of transparent objects for robot hand grasping," in *IROS*, 2021, pp. 5726–5732.
- [33] K. Ohtani and M. Baba, "Shape recognition for transparent objects using ultrasonic sensor array," in *SICE*, 2007, pp. 1813–1818.
- [34] I. Dokmanić and I. Tashev, "Hardware and algorithms for ultrasonic depth imaging," in *ICASSP*, 2014, pp. 6702–6706.
- [35] A. Das, I. Tashev, and S. Mohammed, "Ultrasound based gesture recognition," in *ICASSP*, 2017, pp. 406–410.
- [36] N. Röber, U. Kaminski, and M. Masuch, "Ray acoustics using computer graphics technology," in *Int. Conf. Digital Audio Effects*, 2007.
- [37] K. Takami, T. Furukawa, M. Kumon, and L. C. Ma, "Non-field-of-view indoor sound source localization based on reflection and diffraction," in *MFI*, 2015, pp. 59–64.
- [38] C. Rother, V. Kolmogorov, and A. Blake, "GrabCut" - Interactive foreground extraction using iterated graph cuts," in *SIGGRAPH*, 2004.
- [39] T. Schöps, J. L. Schönberger, S. Galliani, T. Sattler, K. Schindler, M. Pollefeys, and A. Geiger, "A multi-view stereo benchmark with high-resolution images and multi-camera videos," in *CVPR*, 2017, pp. 2538–2547.
- [40] S. Oh, A. Hoogs, A. Perera, N. Cuntoor, C.-C. Chen, J. T. Lee, S. Mukherjee, J. K. Aggarwal, H. Lee, L. Davis, E. Swears, X. Wang, Q. Ji, K. Reddy, M. Shah, C. Vondrick, H. Pirsiavash, D. Ramanan, J. Yuen, A. Torralba, B. Song, A. Fong, A. Roy-Chowdhury, and M. Desai, "A large-scale benchmark dataset for event recognition in surveillance video," in *CVPR*, 2011, pp. 3153–3160.
- [41] D. Leidner and M. Beetz, "Inferring the effects of wiping motions based on haptic perception," in *Humanoids*, 2016, pp. 461–468.
- [42] L. Lu and J. T. Wen, "Human-directed robot motion/force control for contact tasks in unstructured environments," in *CASE*, 2015, pp. 1165–1170.
- [43] J. Kim, A. K. Mishra, R. Limosani, M. Scafuro, N. Cauli, J. Santos-Victor, B. Mazzolai, and F. Cavallo, "Control strategies for cleaning robots in domestic applications: A comprehensive review," *Int. J. Adv. Robot. Sys.*, vol. 16, no. 4, 2019.
- [44] Z. Zhou, X. Chen, and O. C. Jenkins, "LIT: Light-field inference of transparency for refractive object localization," *IEEE RA-L*, vol. 5, no. 3, pp. 4548–4555, 2020.
- [45] D. Tsai, P. Corke, T. Peynot, and D. G. Dansereau, "Refractive light-field features for curved transparent objects in structure from motion," *IEEE RA-L*, vol. 6, no. 4, pp. 6923–6930, 2021.